Thermohaline Structure in the Subarctic North Pacific Simulated in a General Circulation Model*

TAKAHIRO ENDOH

Frontier Research System for Global Change, Yokohama, Japan, and International Pacific Research Center, University of Hawaii at Manoa, Honolulu, Hawaii

HUMIO MITSUDERA

Institute of Low Temperature Science, Hokkaido University, Sapporo, Japan

SHANG-PING XIE

International Pacific Research Center, and Department of Meteorology, University of Hawaii at Manoa, Honolulu, Hawaii

BO QIU

Department of Oceanography, University of Hawaii at Manoa, Honolulu, Hawaii

(Manuscript received 23 April 2003, in final form 7 August 2003)

ABSTRACT

The Miami Isopycnic Coordinate Ocean Model configured with 1° horizontal resolution and 23 layers is used to examine processes that maintain the mesothermal structure, a subsurface temperature inversion, in the subarctic North Pacific. The model successfully reproduces the mesothermal structure consisting of a shallow temperature minimum and an underlying temperature maximum that are called the dichothermal and mesothermal waters, respectively. The mesothermal water is formed through cross-gyre exchange between the subtropical and subarctic gyres, whereas the dichothermal water originates from cold and low-salinity waters formed in the winter mixed layer. The horizontal distribution of the passive tracer injected into the subsurface layers south of Japan shows that warm and saline water of the Kuroshio in the density range of 26.8–27.0 σ_θ is the source of the mesothermal water. There are three pathways through which the Kuroshio waters enter the subarctic region. First, the Kuroshio waters that cross the gyre boundary in the western boundary region are carried to the Alaskan gyre by the northern part of the North Pacific Current. Second, the Kuroshio waters carried by the southern part of the North Pacific Current enter the Alaskan gyre through a cross-gyre window in the eastern basin. Third, the Kuroshio waters that diffuse along the isopycnal in the Kuroshio–Oyashio Extension enter the western subarctic gyre. The mesothermal water thus formed in the subarctic region is entrained into the winter mixed layer and returns to the subtropics as surface water by the southward Ekman drift, forming the subpolar cell.

1. Introduction

A shallow temperature minimum and an underlying temperature inversion are remarkable features in the subarctic North Pacific Ocean (e.g., Dodimead et al. 1963; Uda 1963; Roden 1964, 1977; Favorite et al. 1976; Reid 1973; Ueno and Yasuda 2000). Figure 1 shows typical vertical profiles of temperature and salinity in the subarctic North Pacific. The temperature inversion lies within the strong permanent halocline (hence permanent pycnocline as well). Following Uda (1963), the temperature inversion is called the mesothermal structure, and the waters corresponding to its temperature minimum and maximum are called the dichothermal and mesothermal waters, respectively.

Previous observational studies suggested various processes that maintain the mesothermal structure, as summarized by Ueno and Yasuda (2000). Among them, two main processes are responsible for the creation of the mesothermal structure in the subarctic North Pacific. First, in winter, abundant precipitation, strong cooling, and wind mixing lead to the formation of cold and low-salinity waters, overriding warmer and more saline wa-

* School of Ocean and Earth Science and Technology Contribution Number 6228 and International Pacific Research Center Contribution Number IPRC-223.

Corresponding author address: Dr. Takahiro Endoh, International Pacific Research Center, School of Ocean and Earth Science and Technology, University of Hawaii at Manoa, 1680 East West Road, Honolulu, HI 96822.
E-mail: tendo@hawaii.edu

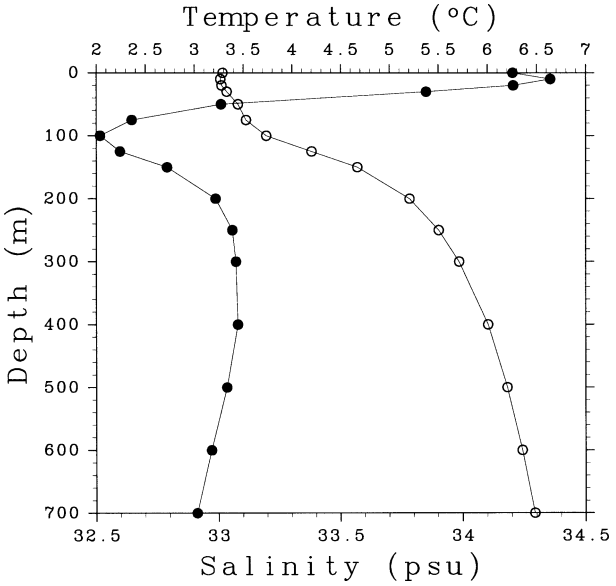

FIG. 1. Vertical profiles of the annual mean potential temperature (solid circles) and salinity (open circles) at 50°N, 165°E (Levitus and Boyer 1994; Levitus et al. 1994).

ters; when surface warming occurs in spring, the dichothermal water is formed between the sea surface and the warm and saline waters (e.g., Uda 1963; Roden 1995; Ueno and Yasuda 2000). Second, differential horizontal advection, in which waters of different temperature and salinity move relative to each other, creates the mesothermal structure. Uda (1963) first suggested that warm and saline waters flowing beneath cold and low-salinity surface waters in the subarctic region form the mesothermal water, although the generation mechanism of such subsurface flow was not explained. Roden (1977) suggested that cold and low-salinity surface waters flowing southeastward under the influence of the southward Ekman drift ride on warm and saline subsurface waters advected by the northeastward geostrophic flow, resulting in formation of the mesothermal structure. This conclusion, however, is based on a one-time hydrographic section restricted in the area from 39° to 47°N and from 158° to 149°W, which is insufficient to identify the origin of the warm and saline waters. Recently, by analyzing the Levitus climatological data, Ueno and Yasuda (2000) showed that warm and saline waters advected from the Kuroshio–Oyashio mixed-water region east of Japan maintain the mesothermal water. In their following paper, Ueno and Yasuda (2001) showed that this result is consistent with high-quality data collected during the World Ocean Circulation Experiment and Subarctic Gyre Experiment. This implies that the mesothermal structure is formed as a part of the ocean circulation of the North Pacific.

In general, numerical models are useful for providing a comprehensive picture of ocean circulation. So far, however, the formation process of the mesothermal structure has not been investigated in the previous numerical models because of their difficulty in reproducing the winter mixed layer in the subarctic North Pacific. Unlike the subtropical gyre where the subduction sets up the upper-ocean stratification, the prevailing Ekman suction in the subarctic gyre acts to push the pycnocline toward the sea surface. This Ekman suction needs to be properly balanced by turbulent mixing in the surface mixed layer whose depth in winter is about 100–200 m in the subarctic North Pacific. Many ocean general circulation models (GCMs) have problems of establishing this balance. The winter mixed layer in the subarctic North Pacific tends to be too shallow (50 m or shallower) in a number of ocean GCMs using various vertical mixing schemes and spatial resolutions. This deficiency is apparent in the GCM simulations of Kunitani (1999) and Xie et al. (2000) using a constant vertical diffusivity, of Ishida et al. (1998) and Qu et al. (2002) using the Pacanowski and Philander (1981) scheme, and of Li et al. (2001) and Chai et al. (2003) using a *K*-Profile Parameterization (KPP) proposed by Large et al. (1994). Not only for the formation of the mesothermal structure, the realistic simulation of the winter mixed layer is also important for the nutrients budget in the subarctic North Pacific, which is in turn important for the spring bloom and hence the regional biogeochemistry (e.g., Chai et al. 2003).

This motivates us to carry out the simulation of the circulation and thermohaline structure in the subarctic North Pacific using the Miami Isopycnic Coordinate Ocean Model (MICOM). MICOM combines a bulk mixed-layer model and a three-dimensional, primitive, isopycnic coordinate model of the stratified oceanic interior. We show that MICOM simulates the winter mixed layer reasonably well in the subarctic North Pacific and proceed to carry out additional experiments to study the formation mechanisms of the mesothermal structure. The purpose of this paper is to document the results from these simulations using MICOM. The sensitivity to the choice of models and/or parameterizations is the subject of our current investigation and will be reported separately.

The paper is organized as follows. Section 2 describes the model and its configuration. Sections 3 and 4 describe the simulated mesothermal structure and the formation of the dichothermal water, respectively. In section 5 we show that the mesothermal structure results from a shallow meridional overturning cell connecting the subtropical and subarctic gyres, and investigate the pathways of this overturning cell. Section 6 provides a summary.

2. Numerical experiment

Figure 2 shows the model domain of our numerical experiment covering the area from 20°S to 63°N and from 120°E to 70°W. We use the gridded bathymetry derived from the 1/12° bathymetric database ETOPO5 (National Oceanic and Atmospheric Administration

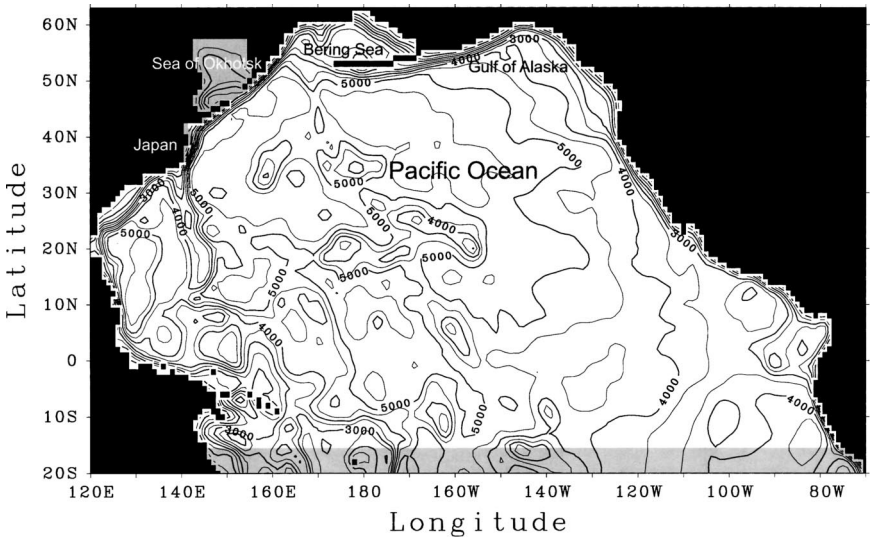

FIG. 2. Model domain and bathymetry. The shaded areas are regions where potential temperature and salinity are restored to the monthly mean climatologies of Levitus and Boyer (1994) and Levitus et al. (1994), respectively. Contour interval is 500 m.

1986) smoothed using a 2° Gaussian filter. Water depths less than 200 m are assumed to be lands, whereas water depths more than 6000 m are assumed to be 6000 m.

The numerical model used in the present study is the MICOM described in detail by Bleck et al. (1992), which combines a bulk mixed-layer model parameterized following the formulation of Gaspar (1988) and a three-dimensional, primitive, isopycnic coordinate model of the stratified oceanic interior. Interior diapycnal mixing is calculated using a scheme developed by McDougall and Dewar (1998). Biharmonic smoothing along isopycnals is applied to suppress small-scale noises. The horizontal grid size Δx is 1° in both latitudinal and longitudinal directions, and there are 23 vertical layers, including a surface mixed layer and 22 isopycnic layers beneath. The values of potential density assigned to these isopycnic layers are 22.0, 22.5, 23.0, 23.5, 24.0, 24.5, 25.0, 25.4, 25.7, 26.0, 26.2, 26.4, 26.6, 26.8, 27.0, 27.2, 27.4, 27.6, 27.70, 27.74, 27.76, and 27.79 σ_θ. The diapycnal diffusivity coefficient K_V is assumed to be inversely proportional to the buoyancy frequency N, and the isopycnal eddy viscosity coefficient A_H and the isopycnal eddy diffusivity coefficient υ_H are assumed to be proportional to Δx. The values of parameters used in the present numerical experiment are $K_V = 1 \times 10^{-7}/N$ (m^2 s^{-1}), $A_H = 0.2\Delta x$ (m^2 s^{-1}), and $\upsilon_H = 0.01\Delta x$ (m^2 s^{-1}). All the lateral boundaries are assumed to be no slip. A quadratic ocean bottom stress is applied with a dimensionless drag coefficient of 0.003.

From a motionless state with a density field calculated from the annual mean potential temperature and salinity data of Levitus and Boyer (1994) and Levitus et al. (1994), the model is driven by the surface wind stress, friction velocity, and heat flux obtained from the monthly mean climatologies of the Comprehensive Ocean–Atmosphere Dataset (Oberhuber 1988; Wright 1988) over 70 yr. The freshwater flux at the sea surface is parameterized by a relaxation of salinity in the surface mixed layer to monthly mean surface salinity of Levitus et al. (1994). Watermass exchange, which occurs between the Sea of Okhotsk and the western North Pacific (Mitsudera et al. 2004; Nakamura and Awaji 2003, manuscript submitted to *J. Geophys. Res.*) as well as outside the model domain, is parameterized by a relaxation of potential temperature and salinity, and hence potential density, to the monthly mean climatologies of Levitus and Boyer (1994) and Levitus et al. (1994) in the shaded areas in Fig. 2. The relaxation time of salinity in the surface mixed layer and that of the density field in the shaded areas are assumed to be 30 and 20 days, respectively. Following Bleck et al. (1989), the contribution of upward buoyancy flux is assumed to be 0.4 times as large as that of downward buoyancy flux. We analyze the calculated results for the final 20 yr.

As an example, Fig. 3 shows the sea surface height (thick lines) as well as the mixed-layer depth (thin lines) in March, the month that the mixed-layer depth in the North Pacific reaches its seasonal maximum. The Kuroshio separates from the Japanese coast north of the observed one because of the coarse horizontal resolution, which causes the mixed-layer depth larger than observed off the eastern coast of Japan (Kobayashi 1999). However, three major gyres, namely, the subtropical gyre, the western subarctic gyre, and the Alaskan gyre, are simulated well. The most significant difference in comparison with the previous numerical studies is that the model successfully reproduces the winter mixed layer deeper than 100 m in both the western subarctic and Alaskan gyres, leading to a more realistic

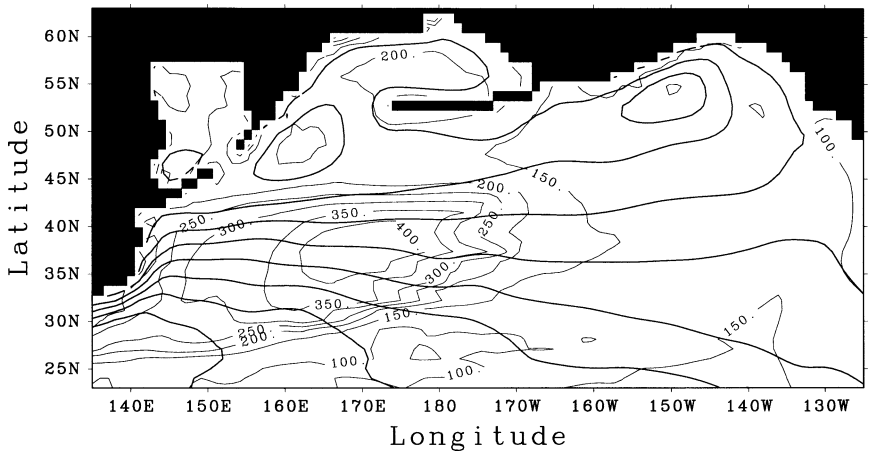

FIG. 3. Sea surface height (thick lines) superposed on the mixed-layer depth (thin lines) in Mar, the month that the mixed-layer depth in the North Pacific reaches its seasonal maximum. Contour intervals are 0.15 m for the sea surface height and 50 m for the mixed-layer depth.

representation of thermohaline structure in the subarctic North Pacific.

3. Distribution of the mesothermal structure

Figures 4 and 5 compare the calculated distributions of potential density and salinity at the depth of the maximum of the annual mean potential temperature with those observed (Ueno and Yasuda 2000), respectively. The distributions in the Sea of Okhotsk, where potential temperature reaches its maximum just above the bottom topography, are not plotted as in Ueno and Yasuda (2000). The general characteristics of the observed mesothermal structure are reproduced well as a whole. The mesothermal structure is distributed north of 45°N, mainly west of the date line where the mesothermal water has a density of 26.8–27.2 σ_θ and a salinity of 33.6–34.0 g kg^{-1}. The density of the mesothermal water increases toward the west from 26.2 σ_θ at 140°W to 27.2 σ_θ at 150°E, also consistent with the observed one.

The mesothermal structures around 50°N east of the date line and along the western coast of North America are not seen in the observed result that is derived from the Levitus climatology. This discrepancy can be attri-

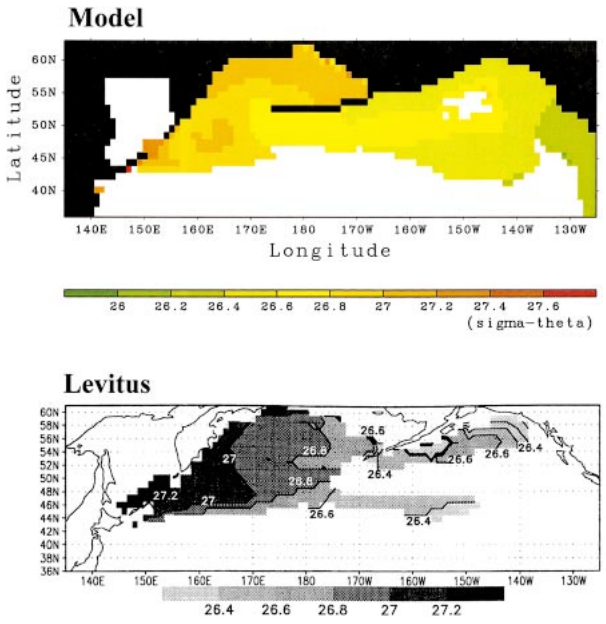

FIG. 4. Comparison of the (top) calculated distribution of potential density at the depth of the maximum of the annual mean potential temperature with the (bottom) observed one adapted from Ueno and Yasuda (2000).

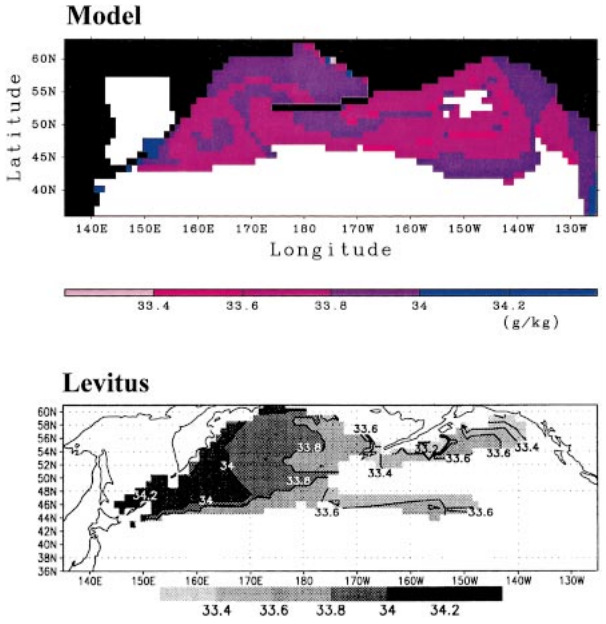

FIG. 5. Comparison of the (top) calculated distribution of salinity at the depth of the maximum of the annual mean potential temperature with the (bottom) observed one adapted from Ueno and Yasuda (2000).

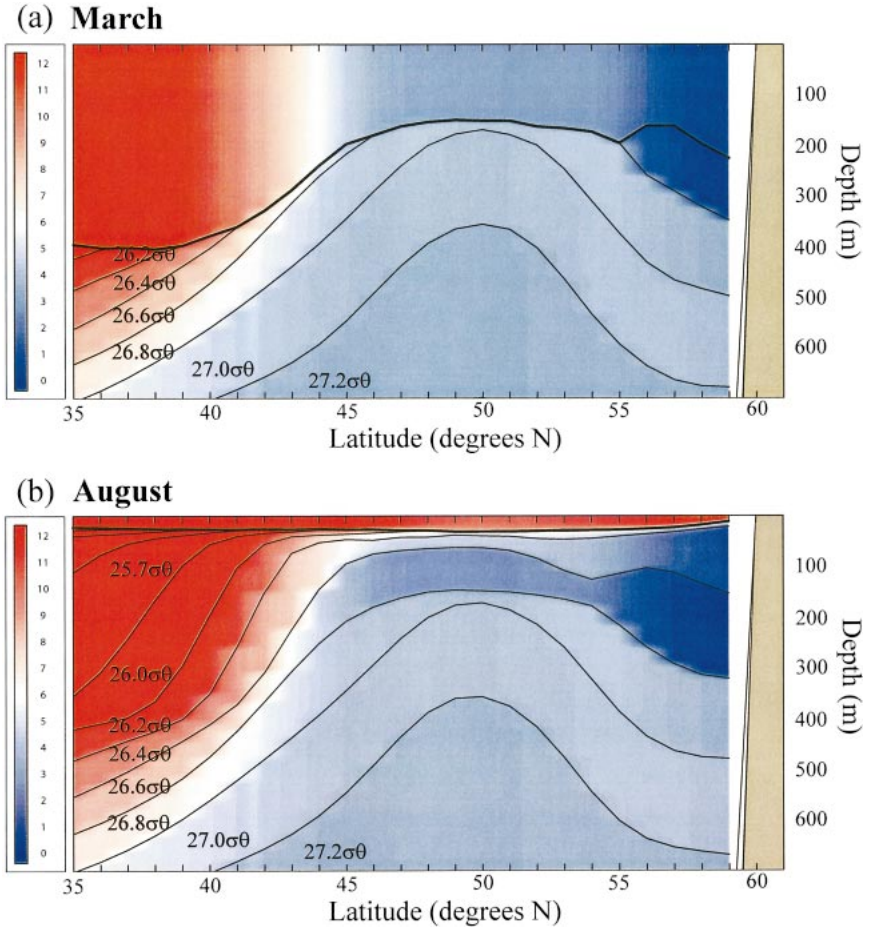

FIG. 6. Vertical structure of layer interfaces (thin lines), the mixed-layer depth (thick lines), and potential temperature (colored contours) along 165°E: (a) Mar and (b) Aug of year 70.

buted to highly spatial smoothing used in the Levitus climatology. Actually, in the raw data of the *World Ocean Atlas 2001*, the mesothermal structure is recognized in these areas (T. Kobayashi 2003, personal communication). To our knowledge, this numerical study is the first to reproduce the mesothermal structure in the subarctic North Pacific.

4. Formation process of the dichothermal water

Figure 6 shows the vertical structures of layer interfaces and potential temperature along 165°E in March and August, the months that represent the extremes of winter and summer conditions in the surface mixed layer. This meridional section runs through the vicinity of the center of the western subarctic gyre, in which the mesothermal structure is mainly distributed (see Figs. 4 and 5). In March, the surface mixed layer deepens above the permanent pycnocline, and only the mesothermal water north of 45°N is present in the depth range of 150–350 m beneath the permanent pycnocline. In August, the seasonal thermocline develops at very shallow depths along the meridional section, resulting in the presence of the dichothermal water in the depth range of 50–150 m over the mesothermal water north of 45°N.

We now describe the calculated results through comparisons with the annual cycle of the observed mesothermal structure. Figure 7 compares the calculated time–depth section of potential temperature at 50°N, 165°E, the vicinity of the center of the western subarctic gyre, with the Levitus climatology. The model reproduces the formation of the dichothermal water very well. In winter, strong radiative cooling and wind mixing coupled with upward buoyancy fluxes lead to deepening of the surface mixed layer to 150 m, where the potential temperature is less than 3.0°C. Over the cold water thus formed, the seasonal thermocline develops during spring and summer as a result of radiative heating and precipitation. Both processes lighten the surface water, thereby forming the dichothermal water underneath the seasonal thermocline. On the basis of the hydrographic data, Miura et al. (2002) proposed a scenario that the dichothermal water in the western subarctic gyre originates from the Bering Sea. In the present numerical model, however,

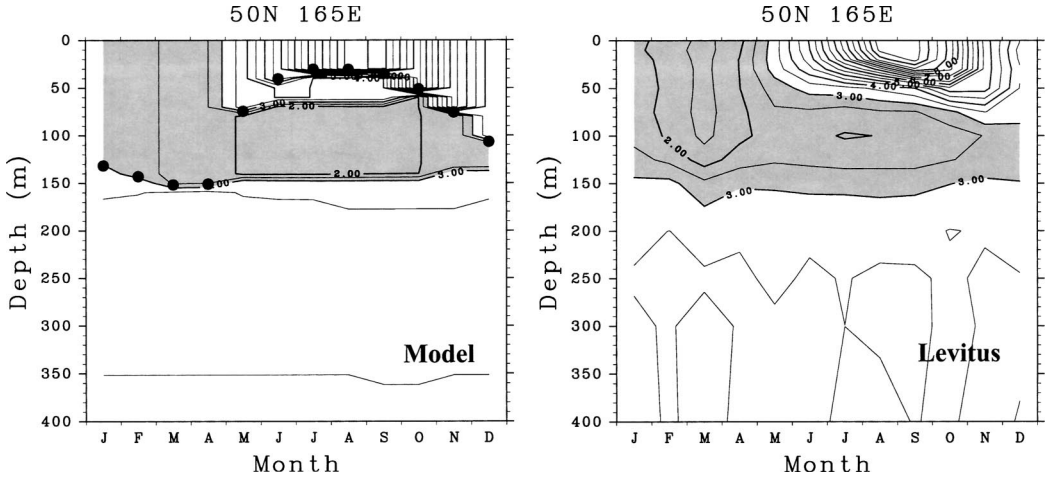

FIG. 7. Comparison of the (left) calculated time–depth section of potential temperature at 50°N, 165°E with (right) the Levitus climatology. The circles trace the evolution of the mixed-layer depth. Contour interval is 0.5°C. Area with the potential temperature less than 3.0°C is shaded.

the dichothermal water originates from cold and low-salinity water locally formed in the winter mixed layer.

It is interesting to note that the layers of 26.8 and 27.0 σ_θ, which correspond to the mesothermal water in the western subarctic gyre, outcrop into the surface mixed layer deepened in winter (in the light and dark shaded areas in Fig. 8, respectively). The potential density in the surface mixed layer is smaller than that of the mesothermal water, consistent with the fact that the isopycnal of 26.8 σ_θ does not outcrop at the sea surface in the North Pacific (e.g., Reid 1965; Talley 1988, 1991, 1993). In addition, the temperature and salinity measurements in winter using the newly deployed Argo profiling float clearly show the deepening of the surface mixed layer just above the mesothermal water in the subarctic North Pacific (Fig. 9). These indicate that the mesothermal water is entrained into the surface mixed layer in winter, a result we further discuss in the next section.

5. Formation process of the mesothermal water

a. The mesothermal water formed as a part of the subpolar cell

Figure 10 shows the annually averaged and wintertime meridional streamfunctions. A shallow overturning cell connecting the subtropical and subarctic gyres is found between 35° and 55°N. The strength of the shallow overturning cell reaches its maximum of 2.6 Sv (Sv $\equiv 10^6$ m^3 s^{-1}) at about 45°N. We hereinafter refer to this overturning cell as the subpolar cell (SPC) pointed out in the numerical study of Lu et al. (1998) using an idealized 3½-layer numerical model. They suggested that the southward Ekman drift across the gyre boundary drives the SPC, generating a subsurface northward flow to balance this surface mass loss. In comparison with the annually averaged meridional streamfunction, the subsurface northward flow of the SPC slightly deepens in winter. Associated with the deepening of the sub-

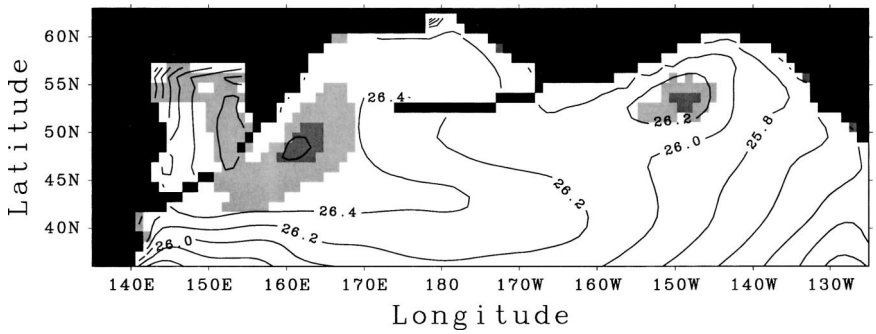

FIG. 8. Potential density in the surface mixed layer in Mar. The light and dark shaded areas are regions where the layers of 26.8 and 27.0 σ_θ outcrop into the surface mixed layer, respectively. Contour interval is 0.2 σ_θ.

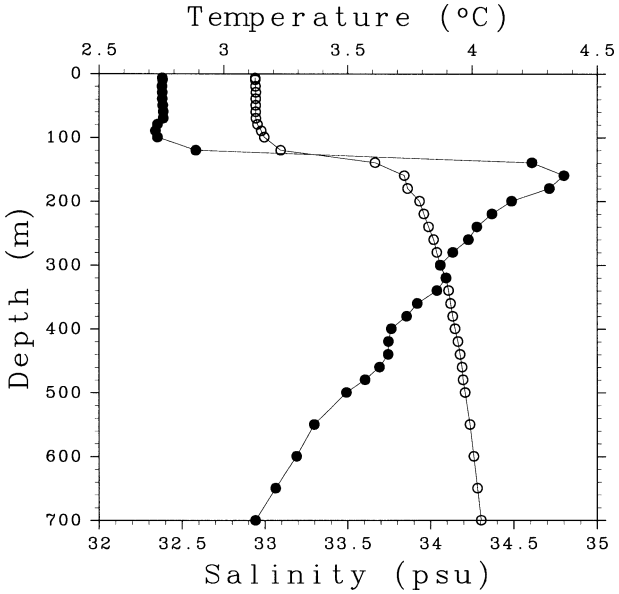

FIG. 9. Vertical profiles of potential temperature (solid circles) and salinity (open circles) observed with an Argo profiling float at 50°40.1′N, 174°13.3′E on 4 Mar 2002.

surface northward flow in winter, the mesothermal water in the density range of 26.8–27.0 σ_θ enters the subarctic region from the subtropics and returns as low-density water in the surface mixed layer. We therefore conclude that the mesothermal structure is an essential part of the SPC.

Figure 10 also shows that almost all waters within the SPC upwell into the surface mixed layer between 45° and 53°N. Lu et al. (1998) attributed upwelling in the subarctic region to Ekman suction. In order to specify the process responsible for upwelling associated with the SPC, we examine the entrainment rate, the flux of fluid entering the surface mixed layer, defined as

$$E = w_{\mathrm{MB}} + \frac{\partial h}{\partial t} + \mathbf{u} \cdot \nabla h,$$

where h is the mixed-layer depth, $\mathbf{u}$ is the horizontal velocity vector in the surface mixed layer, $w_{\mathrm{MB}} = h \cdot \nabla \mathbf{u}$ is the vertical velocity at the base of the surface mixed layer, and t is time (e.g., Cushman-Roisin 1987; Qiu and Huang 1995; Qu et al. 2002). Now we consider the annual mean entrainment rate so that the time variation of the mixed-layer depth $\partial h/\partial t$ can be neglected. Figure 11 shows the contours of annually averaged E, $\mathbf{u} \cdot \nabla h$, and w_{MB} with the contours of the Ekman pumping velocity w_E calculated from the annual mean wind stress. The contribution to the annual mean entrainment rate E from vertical upwelling w_{MB} is predominant north of 45°N except in the Bering Sea and the Sea of Okhotsk where w_{MB} is reduced by lateral induction $\mathbf{u} \cdot \nabla h$. The pattern of the Ekman pumping velocity w_E bears a resemblance to that of w_{MB} in the subarctic North Pacific north of 45°N, except with the opposite sign along the western boundary where convergence of the Oyashio exceeds divergence of the Ekman drift. As a result, in the shaded area from 45° to 53°N and from 156°E to 120°W, the amount of upwelling estimated from w_E (2.6 Sv) is slightly larger than that of the actual upwelling calculated from E (2.5 Sv). The amount of the actual upwelling in this area is nearly equal to the strength of the SPC, indicating that Ekman suction is the dominant mechanism for upwelling in association with the SPC.

b. Source of the mesothermal water

By analyzing the Levitus climatological data, Ueno and Yasuda (2000) showed that heat and salt, advected

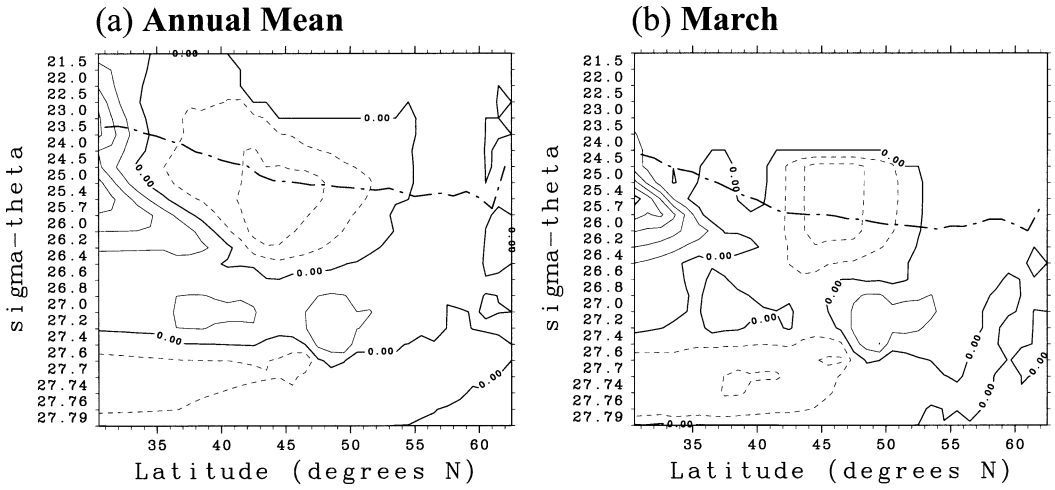

FIG. 10. Contours of the meridional streamfunctions (a) annually averaged and (b) in Mar. Contour interval is 1 Sv. Dashed contours are negative. Dash–dotted line traces the zonally averaged potential density at the base of the surface mixed layer.

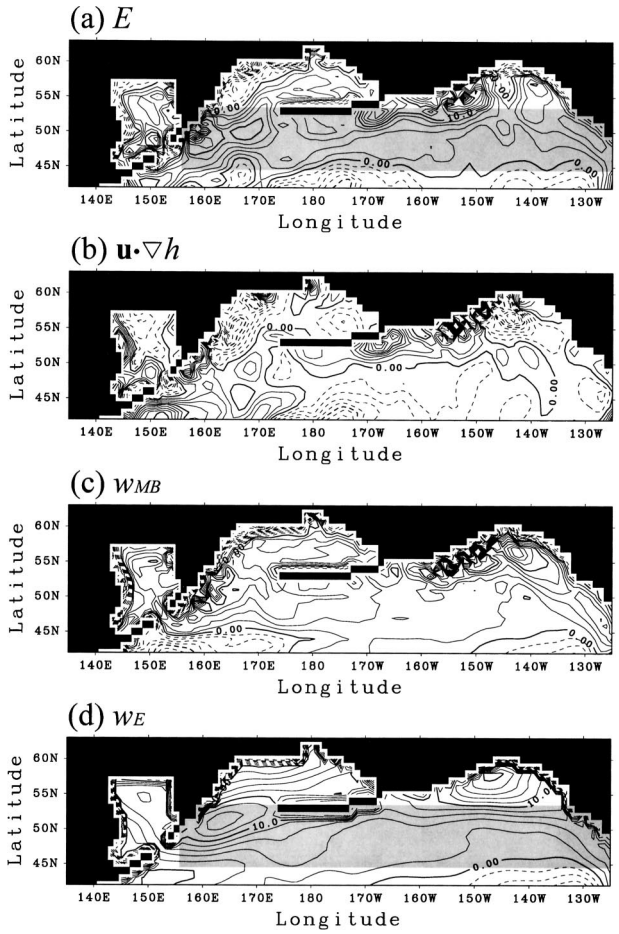

FIG. 11. Contours of annually averaged (a) E, (b) $\mathbf{u} \cdot \nabla h$, and (c) w_{MB} with the contours of (d) w_E calculated from the annual mean wind stress. Contour interval is 2×10^{-7} m s^{-1}. Dashed contours are negative. The shaded areas are used in calculating the amount of upwelling.

from the Kuroshio–Oyashio mixed-water region east of Japan, maintain the mesothermal water in the density range of 26.7–27.2 σ_θ. This suggests that warm and saline water of the Kuroshio is the source of the mesothermal water since the waters in the Kuroshio–Oyashio mixed-water region are strongly affected by the Kuroshio waters. Figure 12 shows the horizontal distribution of the passive tracer continually injected into the layer of 26.8 σ_θ by maintaining the passive tracer south of Japan (in the gray shaded region) at saturation after year 50. The isopycnal eddy diffusivity coefficient for the passive tracer is assumed to be the same as that for potential temperature and salinity. The annually averaged barotropic streamfunction (solid contours) and the gyre boundary (dashed line) derived by subtracting the annual mean Ekman transport from the annually averaged volume transport are superposed. The gyre boundary coincides nearly with the Sverdrup function calculated from the annual mean wind stress except the western boundary region where the Sverdrup balance is no longer satisfied (not shown). It is clear that warm and saline water of the Kuroshio south of Japan is the source of the mesothermal water although most of them flow eastward south of the gyre boundary. The Kuroshio waters that cross the gyre boundary near the western boundary flow eastward along the gyre boundary in the Kuroshio–Oyashio Extension. Some of them spread into the western subarctic gyre after 6 yr, and the others are carried to the Alaskan gyre by the northern part of the North Pacific Current in about 12 yr. We can also see that some of the Kuroshio waters south of the gyre boundary enter the Alaskan gyre west of 150°W after 18 yr.

The effect of the Kuroshio waters on the formation of the mesothermal structure is more directly confirmed in a complementary numerical experiment, in which the influences of the mesothermal structure in the initial density field and water mass exchange between the Sea of Okhotsk and the western North Pacific are completely eliminated. Initial potential temperature and salinity in the depth range of 10–700 m are set to those at the depth of 700 m north of 35°N (Fig. 13a) so that the initial density field does not have the mesothermal structure in the subarctic region. The forcing functions are kept unchanged from the base case except that a relaxation of the density field in the Sea of Okhotsk is not activated. The penetration of the Kuroshio waters into the subarctic region is recognized in the layer of 27.0 σ_θ at year 10 (Fig. 13b). Associated with the penetration, the layers of 26.8 and 27.0 σ_θ continue to thicken (Fig. 13c), and nearly the same mesothermal structure as that in the base case is formed at year 50 (Figs. 6b and 13d) although the mesothermal water is slightly warmer and more saline than that in the base case. This indicates that the Kuroshio waters transferred into the subarctic North Pacific are essential for the formation of the mesothermal structure.

c. *Pathways of the Kuroshio waters from the subtropics to the subarctic region*

To illustrate pathways of the Kuroshio waters from the subtropics to the subarctic region more clearly, a Lagrangian analysis is applied to the annual mean velocity field in the layer of 26.8 σ_θ in the base case. The velocity at the location of the water parcel is determined by using a linear interpolation between the four adjacent grid points. Parcels are released at 36°–39°N, 143°E and tracked by integrating the Lagrangian trajectory equation with a fourth-order Runge–Kutta scheme. Figure 14 shows typical trajectories of two parcels entering the subarctic region and a parcel circulating within the subtropics, labeled A (red), B (blue), and C (green), respectively. Parcel A that enters the subarctic region near the western boundary flows to the Alaskan gyre with the northern part of the North Pacific Current. Lu et al. (1998) and Ueno and Yasuda (2000) suggested that the Kuroshio waters enter the subarctic region via the west-

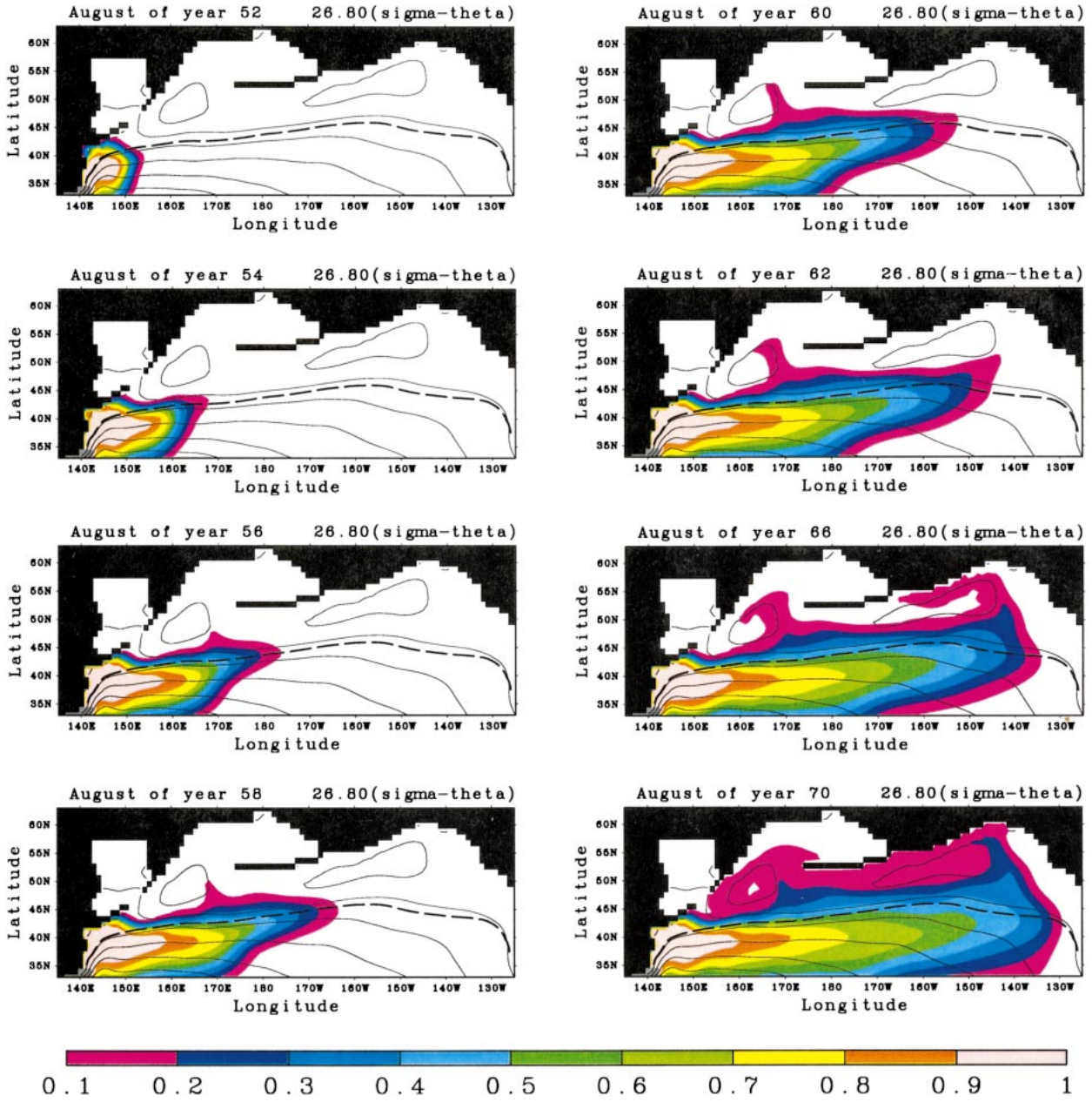

FIG. 12. Horizontal distribution of the passive tracer injected into the layer of 26.8 σ_θ by maintaining the passive tracer at saturation in the gray shaded region after year 50. The annually averaged barotropic streamfunction (solid contours) and the gyre boundary (dashed line) derived by subtracting the annual mean Ekman transport from the annually averaged volume transport are superposed. Contour interval for barotropic streamfunction is 5 Sv.

ern boundary current that compensates the southward Ekman drift in the interior region. In fact, Fig. 15 shows that nearly all of the water mass enters the subarctic region across the western part of the gyre boundary. By contrast, parcel B carried eastward by the southern part of the North Pacific Current enters the Alaskan gyre in the far-eastern basin where the mass flux of the geostrophic flow is almost zero, indicating that this passageway is a cross-gyre ''window'' through which baroclinic exchange between the subtropical and subarctic gyres occurs (Pedlosky 1984; Schopp and Arhan 1986; Schopp 1988; Chen and Dewar 1993; Lu et al. 1998). It should be noted that no parcel enters the western subarctic gyre directly although the passive tracer spreads into the western subarctic gyre. Since isopycnal diffusion is not taken into account in the Lagrangian analysis, we can conclude that the Kuroshio waters diffuse along the isopycnal and spread into the western subarctic gyre while they are carried by the Kuroshio–Oyashio Extension. Indeed, without isopycal diffusion,

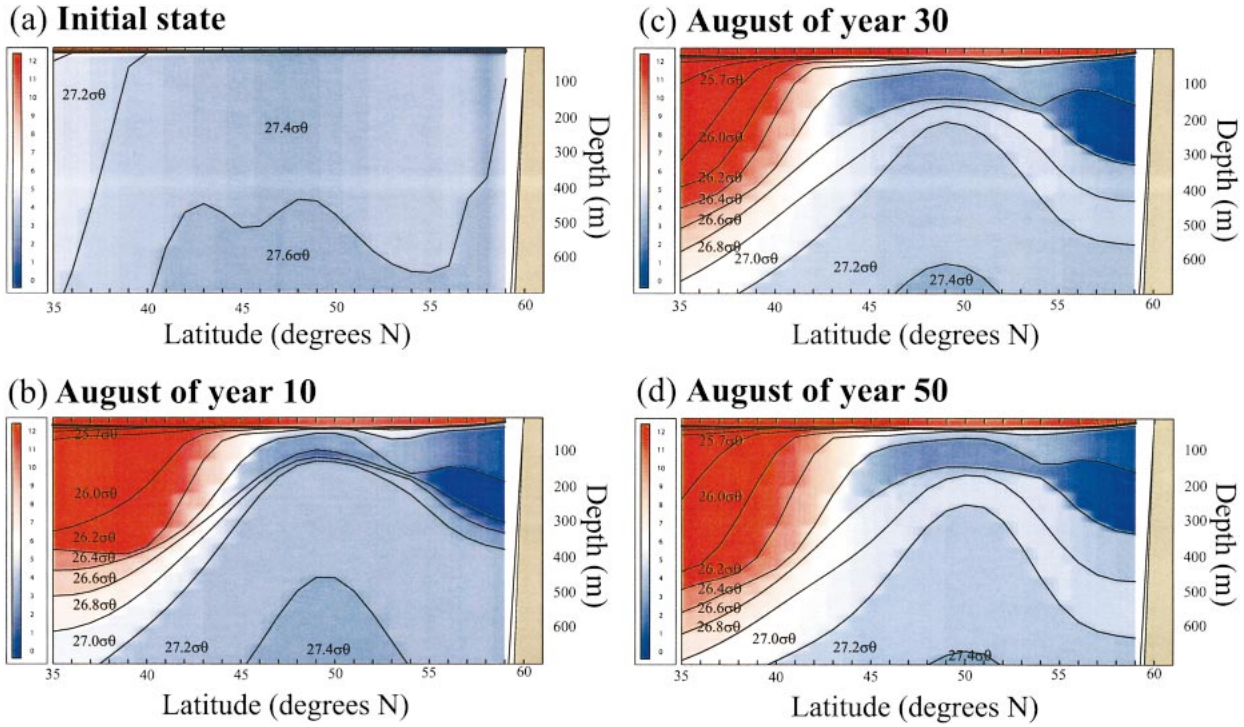

FIG. 13. Same as in Fig. 5 but in the numerical experiment in which initial potential temperature and salinity in a depth range of 10–700 m are assumed to be those at the depth of 700 m north of 35°N: (a) initial state and Aug of (b) year 10, (c) year 30, and (d) year 50.

the passive tracer injected into the same region as in Fig. 12 does not penetrate into the western subarctic gyre (results not shown).

6. Summary

Using the MICOM driven by observed monthly atmospheric climatology, we have successfully reproduced the mesothermal structure, a subsurface temperature inversion in the subarctic North Pacific, consisting of the shallow temperature minimum and the underlying temperature maximum that are called the dichothermal and mesothermal waters, respectively. The dichothermal water originates from cold and low-salinity waters locally formed in the winter mixed layer. In winter, strong surface cooling and wind mixing lead to deepening of the surface mixed layer. Over the cold water thus formed, the seasonal thermocline develops during spring and summer, resulting in formation of the dichothermal water. By contrast, warm and saline water of the Kuroshio in the density range of 26.8–27.0 σ_θ is the source of the mesothermal water. It is suggested that there are three pathways for the Kuroshio waters to enter the subarctic region from the subtropics. First, the Kuroshio

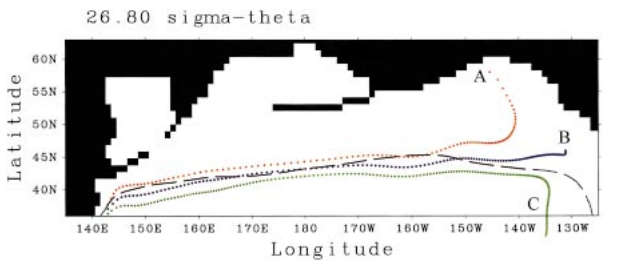

FIG. 14. Lagrangian trajectories for parcels A (red), B (blue), and C (green) superposed on the gyre boundary (dashed line). Each mark is plotted at time increments of 6 months.

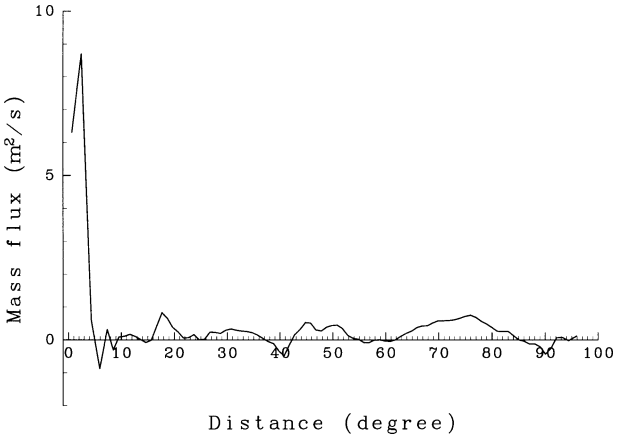

FIG. 15. The annually averaged mass flux of the geostrophic flow entering the subarctic region across the gyre boundary, from which the Ekman flux is excluded. Abscissa indicates the distance along the gyre boundary from the Japanese coast. A three-point triangular smoothing is applied.

waters that cross the gyre boundary in the western boundary region are carried to the Alaskan gyre by the northern part of the North Pacific Current. Second, the Kuroshio waters carried by the southern part of the North Pacific Current enter the Alaskan gyre through the cross-gyre window in the eastern basin. Third, the Kuroshio waters that diffuse along the isopycnal in the Kuroshio–Oyashio Extension enter the western subarctic gyre. The mesothermal water thus formed in the subarctic region is entrained into the winter mixed layer and flows out to the subtropics by southward Ekman drift, forming the SPC.

Several important issues still remain to be investigated. The horizontal resolution used in the present study limited the model's ability to resolve mesoscale eddies and fronts in the Kuroshio–Oyashio mixed-water region. For example, the Kuroshio separating from the Japanese coast north of the observed one coincides with the subarctic front, which might affect the pathway for the Kuroshio waters to the western subarctic gyre. In the presence of mesoscale oceanic features, the Kuroshio waters could also be transferred into the western subarctic gyre by mesoscale eddies that are abundant in the Kuroshio–Oyashio mixed-water region and by the flow along the subarctic front. Sensitivity of the model solution to the choice of vertical mixing parameterization is another area that requires further research. In GCMs with the bulk mixed-layer model, the detrainment process cannot be implemented in a thermal-energy-conserving fashion without sacrificing the accuracy of either mixed-layer depth or mixed-layer buoyancy calculation (Bleck et al. 1989, 1992). The issue of uncertainty in vertical mixing is a major challenge common to all ocean models. This uncertainty may be reduced with better constraints by observations and/or large-eddy simulations (e.g., Wang 2001).

The pathways of the SPC and hence the mesothermal structure may vary interannually. Watanabe (1998) detected significant interannual-to-decadal variations in the distribution of the dichothermal water in the western subarctic gyre, based on the Japanese Salmon Resource Survey in 1966–91 and the data provided by the Japan Oceanographic Data Center. By analyzing the Ocean Topography Experiment (TOPEX)/Poseidon altimetry data, Qiu (2002) found a structural change in the western subarctic gyre from an elongated state in 1993–95 to a contracted state in 1997–99. The observed sea surface height pattern (see his Fig. 17) suggests that the contracted state is likely to facilitate transferring subtropical water mass into the western subarctic gyre, which could have a great impact upon properties of the dichothermal water on interannual time scales. We plan to carry out numerical experiments using a higher-resolution model driven by interannually varying forcing and to investigate the cause of such interannual variability.

The recent Joint Global Ocean Flux Study survey revealed that significant exchange of carbon dioxide between ocean and atmosphere occurs in the subarctic North Pacific (Takahashi et al. 1999). The water exchange between the surface mixed layer and the permanent pycnocline is an important process for nutrients in the euphotic zone, primary production, and hence the ocean uptake of carbon dioxide. As reviewed in the introduction, many ocean GCMs have difficulty in maintaining a deep winter mixed layer as observed in the subarctic North Pacific. An improved simulation of the winter mixed layer as achieved here is certain to have a large impact on simulated biogeochemical cycles in this region, including the nutrient and carbon cycles.

Acknowledgments. This research was supported by the Frontier Research System for Global Change through its sponsorship of the International Pacific Research Center (IPRC). The authors express their gratitude to J. P. McCreary of the IPRC, I. Yasuda and H. Ueno of the University of Tokyo, A. Kubokawa and S. Minobe of Hokkaido University, K. Hanawa of Tohoku University, and T. Kobayashi of the Frontier Observational Research System for Global Change for fruitful discussions. They also thank two anonymous reviewers for their helpful and encouraging comments on the original manuscript. The first author is grateful to Z. Yu, T. Waseda, and Y. Guan of the IPRC, E. Chassignet and G. Halliwell of the University of Miami, and R. Bleck and A. Wallcraft of the Naval Research Laboratory for valuable advice on setting up the numerical experiment.

REFERENCES

Bleck, R., H. P. Hanson, D. Hu, and E. B. Kraus, 1989: Mixed layer–thermocline interaction in a three-dimensional isopycnic coordinate model. *J. Phys. Oceanogr.,* **19,** 1417–1439.

——, C. Rooth, D. Hu, and L. T. Smith, 1992: Salinity-driven thermocline transients in a wind- and thermohaline-forced isopycnic coordinate model of the North Atlantic. *J. Phys. Oceanogr.,* **22,** 1486–1505.

Chai, F., M. Jiang, R. T. Barber, R. C. Dugdale, and Y. Chao, 2003: Interdecadal variation of the transition zone chlorophyll front, A physical-biological model simulation between 1960 and 1990. *J. Oceanogr.,* **59,** 461–475.

Chen, L.-G., and W. K. Dewar, 1993: Intergyre communication in a three-layer model. *J. Phys. Oceanogr.,* **23,** 855–878.

Cushman-Roisin, B., 1987: Subduction. *Dynamics of the Oceanic Surface Mixed Layer,* P. Müller and D. Henderson, Eds., Hawaii Institute of Geophysics Special Publications, 181–196.

Dodimead, A. J., F. Favorite, and T. Hirano, 1963: Salmon of the North Pacific Ocean. Part II: Review of oceanography of the subarctic Pacific region. International North Pacific Fisheries Communication, Bulletin 13, 195 pp.

Favorite, F., A. J. Dodimead, and K. Nasu, 1976: Oceanography of the subarctic Pacific region, 1960–1971. International North Pacific Fisheries Communication, Bulletin 33, 187 pp.

Gaspar, P., 1988: Modeling the seasonal cycle of the upper ocean. *J. Phys. Oceanogr.,* **18,** 161–180.

Ishida, A., Y. Kashino, H. Mitsudera, N. Yoshioka, and T. Kadokura, 1998: Preliminary results of a global high-resolution GCM experiment. *J. Faculty Sci. Hokkaido Univ., Ser. VII,* **11,** 441–460.

Kobayashi, T., 1999: Study of the formation of North Pacific Intermediate Water by a general circulation model and the particle-tracking method, 1, A pitfall of general circulation model studies. *J. Geophys. Res.,* **104,** 5423–5439.

Kunitani, T., 1999: GCM simulation of decadal to interdecadal var-

iability in the North Pacific. M.S. thesis, Graduate School of Environmental Earth Science, Hokkaido University, Japan, 58 pp.

Large, W. G., J. C. McWilliams, and S. C. Doney, 1994: Oceanic vertical mixing: A review and a model with a nonlocal boundary layer parameterization. *Rev. Geophys.,* **32,** 363–403.

Levitus, S., and T. P. Boyer, 1994: *Temperature*. Vol. 4, *World Ocean Atlas 1994,* NOAA Atlas NESDIS 4, 117 pp.

——, R. Burgett, and T. P. Boyer, 1994: *Salinity*. Vol. 3, *World Ocean Atlas 1994,* NOAA Atlas NESDIS 3, 99 pp.

Li, X., Y. Chao, J. C. McWilliams, and L.-L. Fu, 2001: A comparison of two vertical-mixing schemes in a Pacific Ocean general circulation model. *J. Climate,* **14,** 1377–1398.

Lu, P., J. P. McCreary, and B. A. Klinger, 1998: Meridional circulation cells and the source waters of the Pacific Equatorial Undercurrent. *J. Phys. Oceanogr.,* **28,** 62–84.

McDougall, T. J., and W. K. Dewar, 1998: Vertical mixing and cabeling in layered models. *J. Phys. Oceanogr.,* **28,** 1458–1480.

Mitsudera, H., B. Taguchi, Y. Yoshikawa, H. Nakamura, T. Waseda, and T. Qu, 2004: Numerical study on the Oyashio water pathways in the Kuroshio–Oyashio confluence. *J. Phys. Oceanogr.,* in press.

Miura, T., T. Suga, and K. Hanawa, 2002: Winter mixed layer and formation of dichothermal water in the Bering Sea. *J. Oceanogr.,* **58,** 815–823.

National Oceanic and Atmospheric Administration, 1986: ETOPO5 digital relief of the surface of the Earth. National Geophysical Data Center Data Announcement 86-MGG-07, 1 p.

Oberhuber, J. M., 1988: An atlas based on the ''COADS'' data set: The budgets of heat, buoyancy, and turbulent kinetic energy at the surface of the global ocean. Max-Planck-Institut für Meteorologie Rep. 15, 199 pp.

Pacanowski, R., and S. G. H. Philander, 1981: Parameterization of vertical mixing in numerical models of tropical oceans. *J. Phys. Oceanogr.,* **11,** 1443–1451.

Pedlosky, J., 1984: Cross-gyre ventilation of the subtropical gyre: An internal mode in the ventilated thermocline. *J. Phys. Oceanogr.,* **14,** 1172–1178.

Qiu, B., 2002: Large-scale variability in the midlatitude subtropical and subpolar North Pacific Ocean: Observation and causes. *J. Phys. Oceanogr.,* **32,** 353–375.

——, and R. X. Huang, 1995: Ventilation of the North Atlantic and North Pacific: Subduction versus obduction. *J. Phys. Oceanogr.,* **25,** 2374–2390.

Qu, T., S.-P. Xie, H. Mitsudera, and A. Ishida, 2002: Subduction of the North Pacific mode waters in a global high-resolution GCM. *J. Phys. Oceanogr.,* **32,** 746–763.

Reid, J. L., 1965: *Intermediate Waters of the Pacific Ocean.* The Johns Hopkins Oceanographic Studies, Vol. 2, Johns Hopkins Press, 85 pp.

——, 1973: *Northwest Pacific Ocean Waters in Winter*. The Johns Hopkins Oceanographic Studies, Vol. 5, Johns Hopkins Press, 96 pp.

Roden, G. I., 1964: Shallow temperature inversions in the Pacific Ocean. *J. Geophys. Res.,* **69,** 2899–2914.

——, 1977: Oceanic subarctic fronts of the central Pacific: Structure of and response to atmospheric forcing. *J. Phys. Oceanogr.,* **7,** 761–778.

——, 1995: Aleutian basin of the Bering Sea: Thermohaline, oxygen, nutrient, and current structure in July 1993. *J. Geophys. Res.,* **100,** 13 539–13 554.

Schopp, R., 1988: Spin up toward communication between oceanic subpolar and subtropical gyres. *J. Phys. Oceanogr.,* **18,** 1241–1259.

——, and M. Arhan, 1986: A ventilated middepth circulation model for the eastern North Atlantic. *J. Phys. Oceanogr.,* **16,** 344–357.

Takahashi, T., and Coauthors, 1999: Net sea–air CO_2 flux over the global ocean: An improved estimate based on air–sea pCO_2 difference. *Proc. Second Symp. on CO_2 in the Oceans,* Tsukuba, Japan, National Institute for Environmental Studies, 9–15.

Talley, L. D., 1988: Potential vorticity distribution in the North Pacific. *J. Phys. Oceanogr.,* **18,** 89–196.

——, 1991: An Okhotsk Sea water anomaly: Implications for ventilation in the North Pacific. *Deep-Sea Res.,* **38,** 171–190.

——, 1993: Distribution and formation of North Pacific intermediate water. *J. Phys. Oceanogr.,* **23,** 517–537.

Uda, M., 1963: Oceanography of the subarctic Pacific Ocean. *J. Fish. Res. Board Can.,* **20,** 119–179.

Ueno, H., and I. Yasuda, 2000: Distribution and formation of the mesothermal structure (temperature inversion) in the North Pacific subarctic region. *J. Geophys. Res.,* **105,** 16 885–16 897.

——, and ——, 2001: Warm and saline water transport to the North Pacific subarctic region: World Ocean Circulation Experiment and Subarctic Gyre Experiment data analysis. *J. Geophys. Res.,* **106,** 22 131–22 141.

Wang, D., 2001: Large-eddy simulation of diurnal cycle of oceanic boundary layer: Sensitivity to domain size and spatial resolution. *J. Geophys. Res.,* **106,** 13 959–13 974.

Watanabe, T., 1998: Long-term variations in the western North Pacific subarctic gyre. *Long-Term Variability in the North Pacific and Indian Oceans with Implications for Future Observations* (in Japanese), I. Yasuda, Ed., Earth Science and Technology Organization, 30–37.

Wright, P. B., 1988: An atlas based on the ''COADS'' data set: Fields of mean wind, cloudiness and humidity at the surface of the global ocean. Max-Planck-Institut für Meteorologie Rep. 14, 70 pp.

Xie, S.-P., T. Kunitani, A. Kubokawa, M. Nonaka, and S. Hosoda, 2000: Inderdecadal thermocline variability in the North Pacific for 1958–97: A GCM simulation. *J. Phys. Oceanogr.,* **30,** 2798–2813.